Thermochimica Acta, 100 (1986) 223–253
Elsevier Science Publishers B.V., Amsterdam – Printed in The Netherlands

FORTY YEARS IN INSTRUMENTAL THERMOGRAVIMETRY AND MICROCALORIMETRY. CONSEQUENCES IN THE STUDY OF SOLID TRANSFORMATIONS AND FOR CHARACTERIZATION OF THE TEXTURE OF POROUS MATERIALS

C. EYRAUD

Département de Chimie Appliquée et Génie Chimique et Unité Associée au Centre National de la Recherche Scientifique (UA 417), Université Claude Bernard — Lyon I, 43 boulevard du 11 Novembre 1918, 69622 Villeurbanne Cedex (France)

(Received 16 January 1986)

INTRODUCTION

All my research activity took place in Lyon at the University Laboratories Chimie Industrielle (1945–1955), Chimie Minérale (1955–1960), Chimie Appliquée et Génie Chimique (1967–1986) and in the Institut National des Sciences Appliquée (I.N.S.A.) (1960–1967). This research mainly contributed to the study of divided catalytic solids and to the study of transport phenomena through membranes; extensive use was made of thermal analysis, which led us to widen the field of application of well-known techniques, such as thermogravimetry and calorimetry, and to perfect two new methods for analysing the texture of mesoporous solids: thermoporometry and liquid–gas permporometry.

This work was performed in collaboration with the laboratory of Génie Electrique et Ferroélectricité (I.N.S.A. of Lyon) and with two departments of the Commissariat à l'Energie Atomique (C.E.A.): Metallurgy and Isotopic Engineering.

The results are given in an approximately chronological order.

I. THERMOGRAVIMETRY (TGA)

The continuous measurement of weight changes in vacuum or in a controlled atmosphere is a very useful technique for analysing the different steps of preparation of solid catalysts and their evolution with various treatments. An apparatus well adapted for this purpose has been built in our laboratory [1,2]. It comprises a balance, in which the axis of rotation of the beam is on its centre of gravity, the variation in weight of the sample is compensated electromagnetically. The whole system is enclosed inside a metal chamber. This apparatus was marketed in 1958 under the name of

0040-6031/86/$03.50

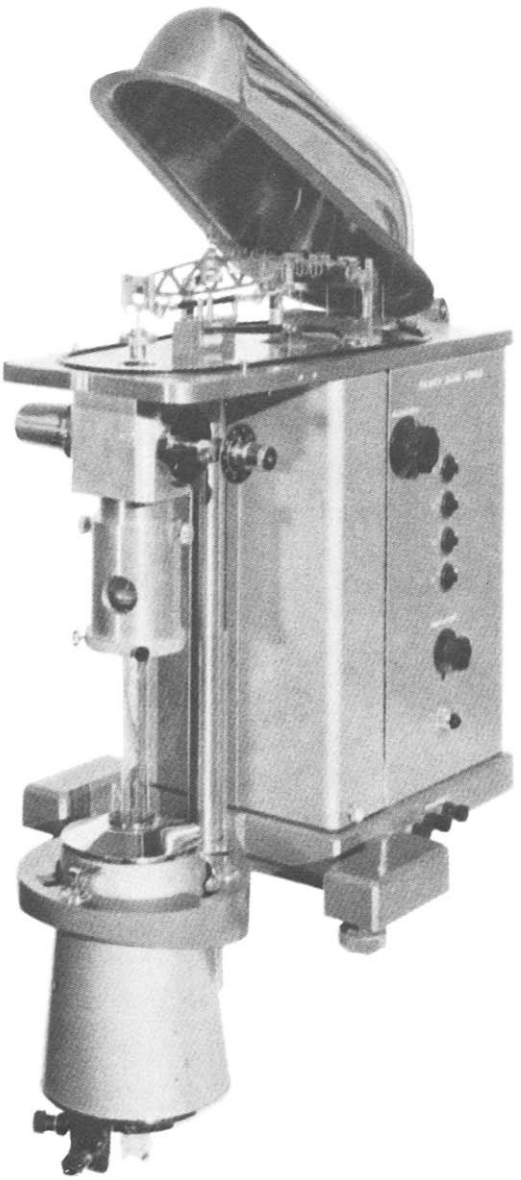

Fig. 1. Ugine-Eyraud balance (type B60).

Ugine-Eyraud (Dam) and improved by the Aram (Fig. 1) and the Setaram companies. Later on, several new models appeared on the market such as Cahn, Mettler, Sartorius, Stanton-Redcroft, Perkin-Elmer, etc. [3].

Thermogravimetry allowed studies of the kinetics of thermal dissociation of alumina hydrates [4], the decomposition in vacuum of hydrated Ni, Co and Mn molybdates [5], the reaction $BaCO_3 + TiO_2 \rightarrow BaTiO_3 + CO_2$ [6], the carburization of nickel by CO [7] or by hydrocarbons [8], the evolution

of a copper oxide catalyst during the oxidation reaction of isopropyl alcohol in acetone [9], the isosteric heat of adsorption of water on oxides [10], water adsorption by A-type molecular sieves [11], the surface area of a bi-metallic catalytic phase (Pt–Re or Pt–Ir) by oxidation or reduction of chemisorbed gases (H_2, O_2) [12].

For such a large variety of experiments, in order to limit the possibilities of errors on weight and temperature measurements or to avoid the penetration of corrosives or condensable gases into the moving part of the balance, the enclosure surrounding the sample pan has to be adapted for each case [13,14].

The surface area of a divided iron fluoride, made by combustion of the anode of an electric arc in fluor [15], or by the reaction of fluor and iron pentacarbonyl in a flame [16], can be determined by the BET method using gravimetric measurement of the amount of gas adsorbed. From these sorption measurements it is possible to determine the pore size distribution according to the BJH method (BJH porometry) [17] and to follow the evolution of the texture of a solid at each step of a thermal treatment without allowing the sample to come into contact with air.

The thermobalance is an apparatus well suited to the determination of the magnetic susceptibility of various samples such as divided carburized nickel [7], chromium oxide on silica–alumina catalysts [18], cupric oxide [19], Mo and Co mixed sulphurs [20] or clay-containing substituted Fe^{2+} ions submitted to a dehydroxylation treatment [21].

The molar energy of adsorption of water on various clay materials as a function of the hydration degree has been measured by coupling a B60 balance with an Eyraud–Richard [22–24] microcalorimeter.

II. ADIABATIC CALORIMETERS AND FLUXMETERS

Some studies performed in our laboratory make use of the determination of the amount of heat produced by an electrical process, a luminous source or a chemical reaction. Therefore, we have been led to design new thermal analysis devices.

II.1. Energetic yield in the synthesis of NO in a high frequency arc

Forty years ago, publications [25] and patents indicated an abnormally high energetic yield in the synthesis of NO in the high frequency electric arc. Since we suspected an erroneous measurement of the current–voltage phase difference, we immersed the electrical reactor into a calorimeter filled with 10 l of paraffin. We were therefore able to show that the energetic yield of this reaction was the same with direct, alternating (50 Hz) or high frequency currents (2–20 MHz) [26,27]. Moreover, the temperatures of the various

zones of discharge of the arc were measured using a spectroscopic method [28] derived from that used in astronomy. These results put an end to the hope created in chemical industry by the initial publications.

II.2. Energetic and topochemical aspects of the combustion of methane on incandescent platinum

The apparatus most commonly used to determine the amount of methane in the atmosphere of a coal mine is based on the catalytic combustion of the hydrocarbon on an incandescent platinum wire. This wire, which is part of a Wheatstone bridge, is heated at 1000°C by the Joule effect. The temperature rise produced by the heterogeneous reaction at the surface of the platinum produces a variation of the electrical resistance which is proportional to the amount of combustible gas. This device presents two drawbacks: the change in catalytic activity of platinum and the drift of the equilibrium point. Three aspects of this problem have been studied: the role of the chemical reaction on the rate of vaporization of platinum, the occurrence of a homogeneous reaction taking place along the heterogeneous reaction of oxidation and the crystallographic evolution of platinum with time.

(a) By using an irradiated platinum foil and by measuring the radioactivity of the gas issued from the combustion of 3% of methane in air, at a constant temperature of 1250°C, we have shown that the rate of evaporation of platinum is four times higher than when no reaction occurs [29]. The combustion yield is 80%.

(b) With simultaneous measurement of the potential difference and the intensity it is possible to find the electrical energy necessary to keep the catalyst at constant temperature, whatever the chemical process being studied. It is therefore possible to deduce the energy transferred to the catalyst by the chemical reaction. We noticed that a large proportion of the energy produced by the reaction was dissipated far from the surface of the catalyst. [30].

(c) By allowing either methane or oxygen to be in contact with the platinum we could see that only oxygen was activated by platinum and that the oxygen activated by this process could induce homogeneous combustion of a fraction of the mixture [31].

(d) We have postulated that the grain boundaries of the metal, which are zones of important atomic disorder, can constitute defects sensitive to a direct electrical current. We have been able to observe a rapid electromigration of the grain boundaries in several metals (Ag, Co, Cu, Ni, Au, Pd, Pt) at a temperature close to their melting points [32–35]. A twin crystal junction can be used as a fixed mark as long as it is not "rubbed out" by a moving grain boundary. The pressure exerted on the grain boundary by the electrical current can be considered as the sum of two terms: a pressure due to the electric field, directed towards the anode; and a pressure due to the diffusion

of the electron, directed towards the cathode. The resulting displacement takes place in the direction of the anode or cathode according to the nature of the metal and of the impurities. The rate of the process is ~ 10–20 cm h^{-1} for electrical fields in the range 20–100 V m^{-1}, and increases with current density. The groove produced by evaporation of the metal slows down the displacement whereas the superficial mobility, which is a function of temperature, accelerates it. This phenomenon, which had never been observed previously, is very important in microelectronics. It has been illustrated by a film.

II.3. Enthalpimeters

The Tian–Calvet calorimeter allows continuous measurement of very small thermal effects taking place over several days with an accuracy better than a microwatt. It is a calorimeter operating in quasi-isothermal conditions. In order to perform measurements in non-isothermal conditions it is possible to devise a less sophisticated apparatus. For determination of the enthalpy of dehydration of hydrargillite [36], of polymorphic transformations of silica [37] or the congealation of capillary condensates [38], we conceived a differential thermal analysis apparatus with electrical energy compensation [39]. Due to the necessity of determining the thermal properties of beryllium and for studying the texture of mesoporous filters in a work under contract with the Atomic Energy Commission (CEA), I asked Professor L. Eyraud of the Laboratory of Ferroelectricity (INSA) to study more accurate apparatuses under the name of "enthalpimeters". The basis is a fluxmeter made of two cells associated to form a differential captor. The system is embedded in refractory cement, which does not undergo any transformation within the range of temperature under study, and is placed inside a block made of copper, stainless steel, alumina or beryllium oxide assuring the best possible temperature homogeneity. The differential captor is made of multi-thermocouples [40–42] as shown in Fig. 2 or thermoresistors made with coils of platinum wire [43] (Fig. 3).

II.4. Thermal properties of bulk beryllium oxide

The manufacture of beryllium bricks by hot pressing was part of a project to build a high temperature nuclear reactor. We were asked to determine the Wigner energy of samples irradiated by neutrons and to measure thermal diffusivity coefficients up to 1000°C.

II.4.1. Wigner energy in BeO

The direct measurement of Wigner energy in BeO presents two difficulties which cannot be overcome by usual thermal analysis methods. The recovery of this material irradiated by neutrons is an example of an irreversible

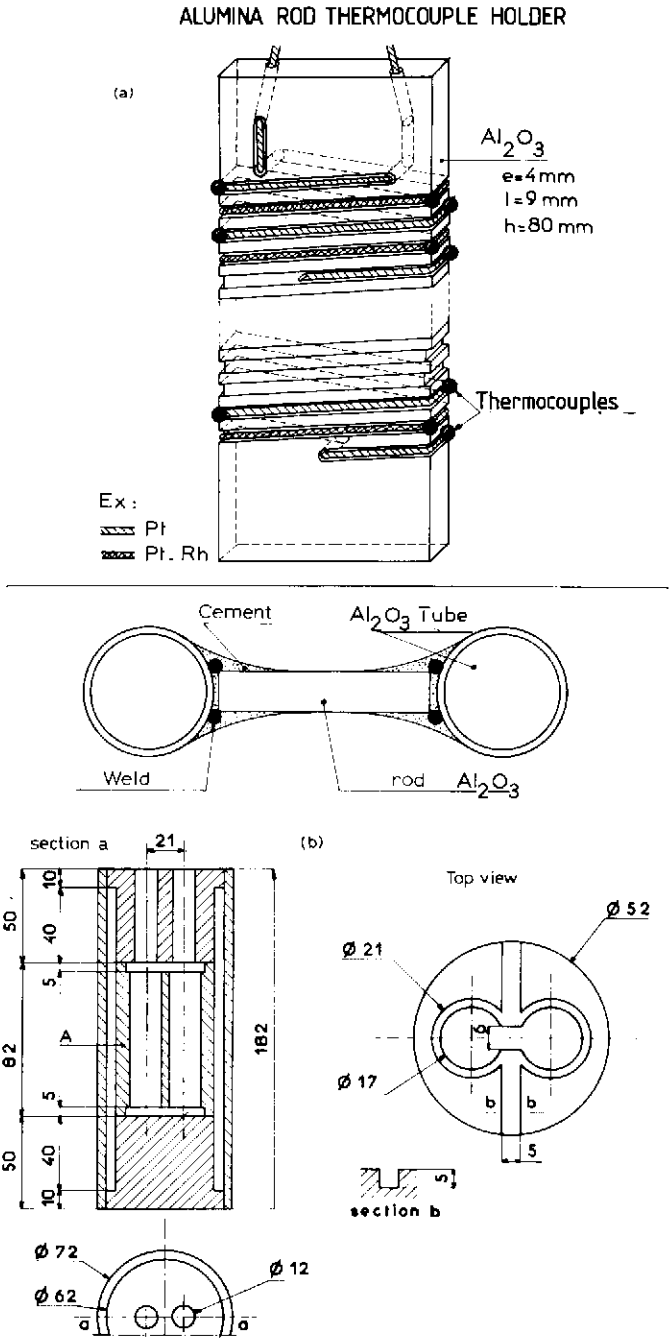

Fig. 2. (a) Thermocouple detector for the quantitative differential thermal analysis device. (b) Calorimetric block for the quantitative differential thermal analysis device.

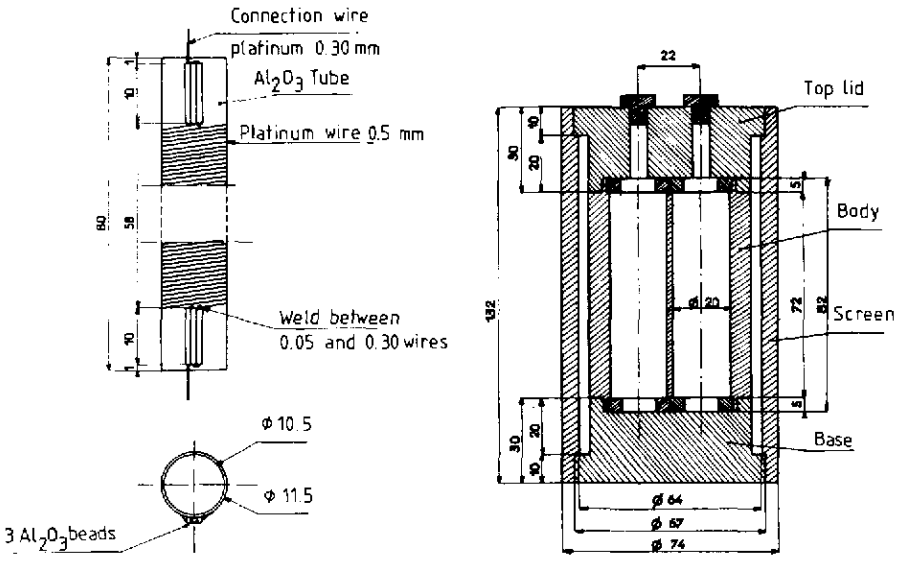

Fig. 3. (Left) Thermoresistor detector for the quantitative differential thermal analysis device. (Right) Calorimetric block for the quantitative differential thermal analysis device.

transformation in which the energies involved are very small and spread over a very large temperature range. These conditions necessitated a new device based on an isothermal ballistic method with compensation. The calorimeter block made from BeO (Eyraud–Richard) is heated at 1200°C. The sample which was previously kept in an isothermal enclosure above the calorimeter is lowered at constant speed inside the laboratory cell. The same operation is performed with the recovered sample (Fig. 4). The recovering energy is obtained by the difference between the two thermal analysis curves. In order to improve the sensitivity of the method a compensation of the useless area corresponding to the heating of BeO is performed by the use of an electrical device acting on the thermoelectric cell [44]. For BeO samples, which have been submitted to irradiation between 0.6×10^{19} and 4×10^{19} n_r cm^{-2} (neutrons of energy above 1 MeV) at a temperature less than 100°C, the Wigner energy (measured between 50 and 1200°C) is between 100 and $175 \pm 15\%$ cal mol^{-1} BeO. The energy stored by MgO, SiO_2 and Al_2O_3 irradiated by neutrons has been also measured [45].

II.4.2. Measurement of the thermal diffusivity of bulk BeO up to 1400°C

One method involves the production of a sinusoidal thermal attack on the plane side of a parallelepipedic sample with the help of a platinum resistor [46] or of an image furnace [47]. Two thermocouples are placed at distances x_1 and x_2 from the side, respectively. The ratio of the amplitudes or of the phase differences of the two alternative components of the temperatures at the points x_1 and x_2 allows calculation of the thermal diffusivity coefficient.

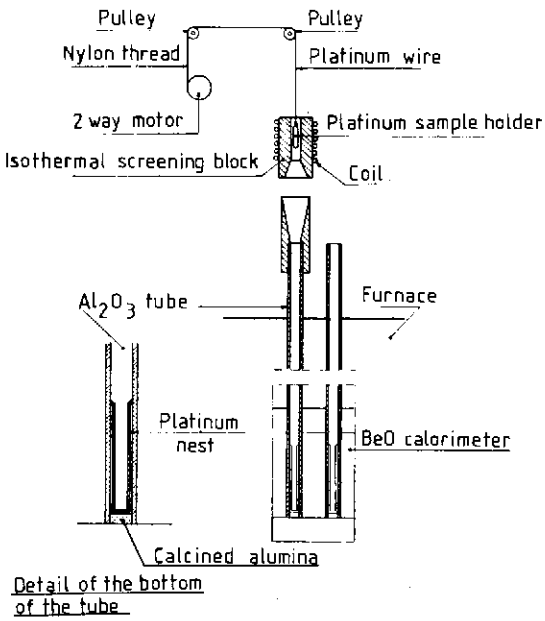

Fig. 4. Differential drop calorimeter.

When the solid does not undergo any phase change the curve giving the variation of the thermal diffusivity coefficient does not present any singularities. This is the case for BeO in the temperature range 50–1000°C. In the case of barium titanate a discontinuity is observed at 120°C corresponding to the tetragonal to cubic transformation [48]. The solution of the Fourier equation is not known in the case where the thermal conductivity coefficient is a function of temperature. An approximate solution can give an estimation of the error on the experimental determination of the thermal diffusivity coefficients [49].

Another method involves submitting the sample to a thermal shock. Three detectors in suitable places give information on the propagation of the perturbation and eventually of the solid–solid transformation energies. Thermal diffusivity coefficients have been determined in this way for BeO between 200 and 1400°C and for Al_2O_3 between 200 and 1200°C [50,51].

III. THERMOPOROMETRY

We have been interested in producing mesoporous ultra-filters (usually of cylindrical shape), which can be classified as one of the following types: homogeneous elements, elements with thick separative layer (10–100 μm), elements with thin separative layer (1–10 μm). In the first and second cases the active layer can be separated from its support and the pore size

distribution determined by mercury porometry or by BJH porometry. The first method is based on the mechanical equilibrium of the interfaces (Laplace equation) but is limited to solids which cannot be deformed by the pressure required to force mercury into the pores [52]. The second method is based on the mechanical and physicochemical liquid–vapour equilibrium described by the Kelvin equation. Sorption isotherms are obtained by using a more or less automated apparatus by volumetric [53] or gravimetric [17,54] methods.

The calorimetric study of the liquid → solid transformation of a capillary condensate saturating a porous material provides a new method for the characterization of texture. The apparatus used for the first attempt was not sophisticated enough [38], and it was necessary to allow the team of Prof. L. Eyraud to study and build the very sensitive enthalpimeters suitable for our purpose (see section II.3). The method called thermoporometry is especially suitable for the study of materials which cannot undergo compression or drying without modification of texture. Moreover, the novelty of this method with respect to the other methods of study of porous structures is that, instead of giving the radius of the opening, it gives an analysis of the inside of the pore. This method can be successfully used for pore radii within the range 1.5–150 nm.

III.1. Theoretical background

The method is based on the thermodynamic relationship of the solid–liquid–vapour equilibrium of a capillary condensate. The average radius of curvature R_{12} of the interfaces formed inside the mesoporous body causes a pressure difference ΔP_{12} between the two phases, 1 and 2. This difference is given by the Laplace equation:

$$\Delta P_{12} = P_1 - P_2 = \frac{2\gamma_{12}}{R_{12}} \tag{1}$$

This equation expresses the mechanical equilibrium of an interface of surface energy γ_{12} per surface unit. R_{12} has a positive value if the concavity of the surface is facing phase 1.

III.2. Phase rule

When all the interfaces are flat, the system consisting of three phases of a pure compound is invariant. This system exists only at a temperature T_0 which is called the triple point temperature.

When the interfaces are no longer flat, their curvatures become state variables of the system. Therefore, if we consider the case of a pure compound held inside a conical-shaped pore as shown in Fig. 5, the three phases are in equilibrium at a temperature T, different from T_0. If the

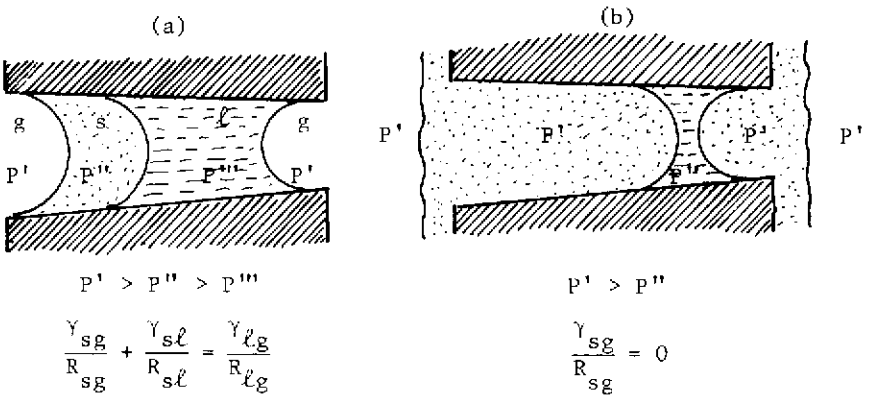

Fig. 5. Equilibrium of the three phases of a condensate inside an cylindrical capillary.

pressure is considered to be uniform throughout the same phase, the curvatures of the three meniscuses follow the equation:

$$\frac{\gamma_{sg}}{R_{sg}} + \frac{\gamma_{sl}}{R_{sl}} = \frac{\gamma_{lg}}{R_{lg}} \tag{2}$$

The variance of the system is now 2. Let us write the Gibbs-Duhem equations for each phase and the Laplace equation for each interface

$$\begin{aligned} -s_g\,\mathrm{d}T + v_g\,\mathrm{d}p_g &= \mathrm{d}\mu & p_s - p_g &= \frac{2\gamma_{sg}}{R_{sg}} \\ -s_l\,\mathrm{d}T + v_l\,\mathrm{d}p_l &= \mathrm{d}\mu & p_l - p_g &= \frac{2\gamma_{lg}}{R_{lg}} \\ -s_s\,\mathrm{d}T + v_s\,\mathrm{d}p_s &= \mathrm{d}\mu & p_s - p_l &= \frac{2\gamma_{sl}}{R_{sl}} \end{aligned} \tag{3}$$

Combination of these equations [55] gives the following differential equation:

$$\left(W_{solid} + \frac{v_l - v_s}{v_g} W_{subl}\right) \frac{\mathrm{d}T}{T} = v_l\,\mathrm{d}\frac{2\gamma_{sl}}{R_{sl}} - (v_l - v_s)\,\mathrm{d}\frac{2\gamma_{sg}}{R_{sg}} \tag{4}$$

As $v_l - v_s$ is very small the term containing the sublimation energy can be disregarded. A further simplification of eqn. (4) is obtained if the total volume of liquid is larger than that of the pores [56,57]. In this case at the temperature T_0 of the normal triple point, the solid–gas interface is flat and $2\gamma/R_{sg} = 0$. The variance of the system is then 1. The simplified equation obtained is either:

$$\frac{\mathrm{d}T}{T} = \frac{2v_l}{W_S}\mathrm{d}\frac{\gamma_{sl}}{R_{sl}} \text{ or } \mathrm{d}T = 2\frac{v_l}{\Delta S_S}\mathrm{d}\frac{\gamma_{sl}}{R_{sl}} \tag{5}$$

or in the integral form:

$$\Delta T = \int_0^{(\gamma_{sl}/R_{sl})} \frac{2v_l}{\Delta S_S} \mathrm{d}\frac{\gamma_{sl}}{R_{sl}} \tag{6}$$

$\Delta T = T_0 - T$ is the decrease of the triple point temperature as a function of the radius of curvature, R_{sl}.

ΔS_S is the solidification entropy of the bulk phase, given by:

$$\Delta S_S = \Delta S_{S_0} - \frac{1}{T}\int_{T_0}^{T} \frac{C_l - C_s}{T}\mathrm{d}T - \frac{2}{T}\int_0^{(\gamma_{ls}/R_{sl})} \left[\frac{v_s}{v_s - v_l}\left(\frac{\partial v_l}{\partial T}\right)_p - \frac{v_l}{v_s - v_l}\left(\frac{\partial v_s}{\partial T}\right)_p \right] \mathrm{d}\frac{\gamma_{ls}}{R_{sl}} \tag{7}$$

ΔS_{S_0} is the normal solidification entropy, C_l and C_s are the heat capacities of the liquid and solid, respectively.

For a given condensate a good approximation of ΔS_S can be obtained from the expression of C_l and C_s as a function of temperature.

III.3. Determination of pore radii by thermal analysis

The previous relationship theoretically allows the determination of a pore radius r by measuring ΔT provided the radius of curvature R_{sl} of the interface is univocally related to this pore radius.

Let us consider the porous structure shown in Fig. 6. The crystallization of a liquid (l) into a solid (s) or of a solid s_1 into a solid s_2 can take place by nucleation (pore A), by penetration (pore B) or by both mechanisms successively (pore C). As a result, the mechanism of change of state of a capillary condensate must depend on the direction of the temperature variation and on the shape of the pores.

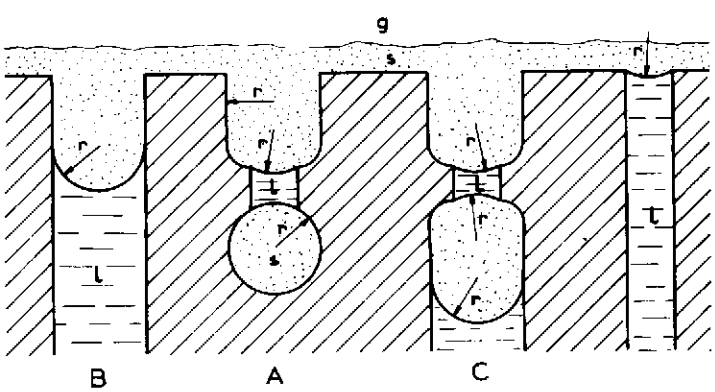

Fig. 6. Equilibrium of the three phases of a condensate inside a porous solid.

We will consider the case of two typical pore structures: cylindrical pores and spherical cavities with small openings.

III.3.1. Cylindrical pores

The pore radius is expressed as a function of the radius R of the interface and of the contact angle θ by the equation (Fig. 7a):

$$r = R \cos \theta \tag{8}$$

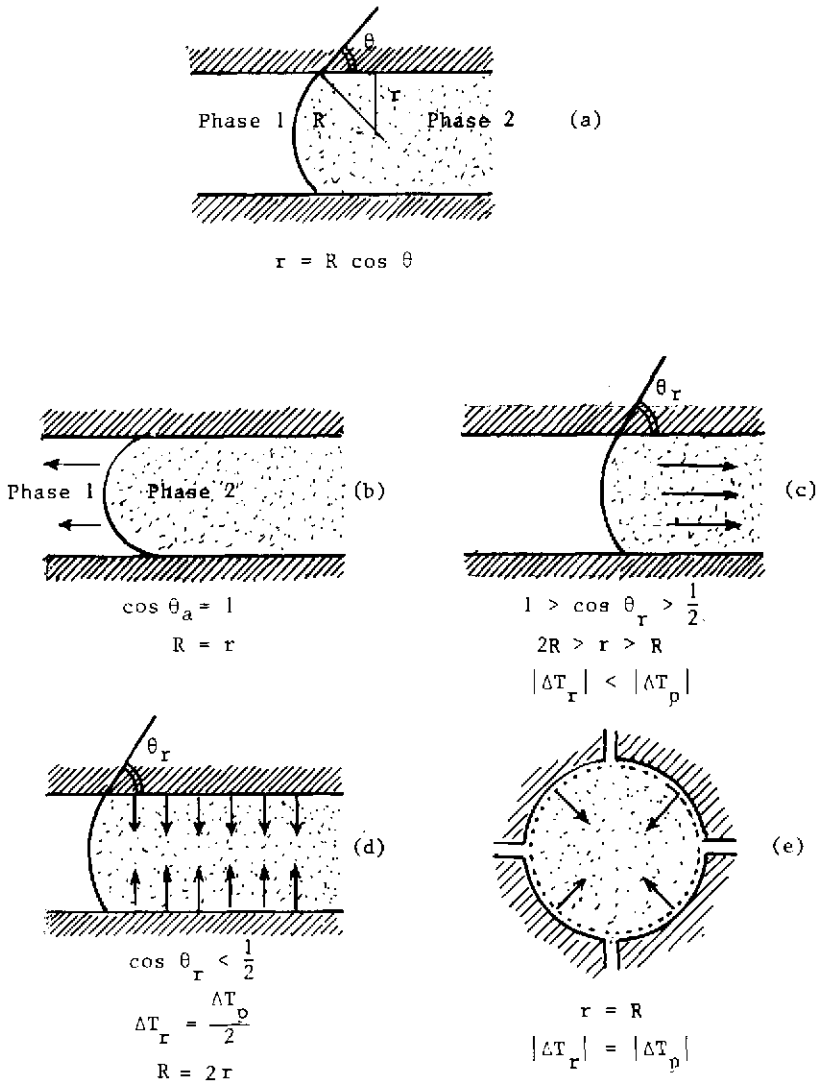

Fig. 7. Evolution of the solid–liquid interface of a condensate on decreasing and increasing the temperature, respectively.

Assuming that the contact angle depends on the direction of motion of the meniscus [58], when the temperature is decreased phase 1 changes into phase 2 and the meniscus advances with a minimum contact angle θ_a. Experimental studies of the solidification of water, benzene [59] or carbon tetrachloride [60] inside a porous body of known pore radius, show that θ_a is approximately zero (Fig. 7b).

When the temperature is increased the meniscus recedes and the contact angle θ_r increases. The curvature and therefore the diminution of the triple point temperature are smaller than when the temperature is increased: $|\Delta T_r| < |\Delta T_a|$.

The receding of phase 2 is controlled by the curvature of the meniscus as long as $\cos \theta_r > 1/2$ (Fig. 7c). When $\cos \theta_r < 1/2$ the receding of phase 2 is then controlled by the average curvature of the pore.

The cylinder of phase 2 acts as the nucleus and $|\Delta T_r| = |\Delta T_a|/2$ (Fig. 7d). Such a behaviour is observed for many organic liquids and for water

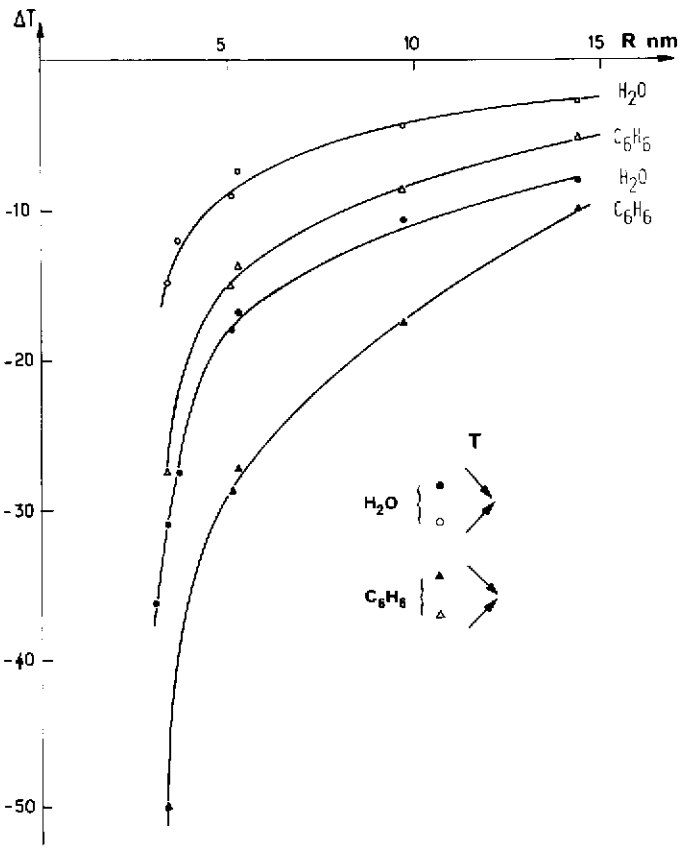

Fig. 8. Depression of the freezing and melting points of water and of benzene as a function of the pore radius.

saturating mesoporous grains obtained by high temperature treatment of γ-alumina [61,62,63].

The theoretical hypothesis can be verified by measuring the decrease of the triple point temperature of condensates inside well-calibrated cylindrical pores. Figure 8 [56] shows that the diminution of the triple point temperature for solidification is approximately half the corresponding diminution for melting of water as well as for benzene.

III.3.2. Cavities

For spherical cavities connected by openings with very small radii, the conditions of formation and of disappearance of the nuclei are the same: therefore $\Delta T_r = \Delta T_a$ and the thermograms must be the same during cooling and heating. This is what is observed for samples obtained by compression of non-porous particles without sintering [60,61].

Between these two extreme cases corresponding either to Fig. 7d or to Fig. 7e, it is possible to imagine many configurations.

In the case of a narrow pore size distribution it is possible to define a simplified shape factor:

$$f = \frac{\Delta T_a}{\Delta T_r} \text{ with } 1 < f < 2 \tag{9}$$

For a large pore spectrum, a "thermodynamic shape factor" f_t is defined; its value is also between 1 and 2 [57].

The pore size is given by eqn. (5) for liquid–solid transformations only, as the curvature is then related univocally to the pore radius.

Figure 9 shows a plot of the values of $1/\Delta T$ as a function of r measured on material with a narrow pore size distribution of cylindrical pores of known average radius between 3.0 and 10 nm.

The linear dependence indicates that the ratio $\gamma_{sl}/\Delta S_{sv}$ is not noticeably dependent on temperature. ($\Delta S_{sv} = \Delta S_{sv}/v_l$ is the volumetric variation of entropy for the solidification.)

Intersection of the lines with the abscissa axis gives the value of t which is the thickness of the layer of the condensate which is not transformed. Therefore, $r = r_n + t$. The value of t obtained by thermal analysis is in good agreement with the values deduced from calorimetric measurements.

As a conclusion, only the liquid → solid transformation can be used in order to perform a "thermoporometry".

Nevertheless, it is possible to obtain useful information about the shape of the pores if each part of the crystallized condensate can be considered to be a nucleus trapped inside the porous matrix.

The nucleus is probably protected from strong solid–matrix interactions by the layer of molecules of condensate which retains liquid-like properties. We will see later that the existence of this interphase is necessary in order to interpret the results of calorimetric measurements. The "trapped nuclei" are

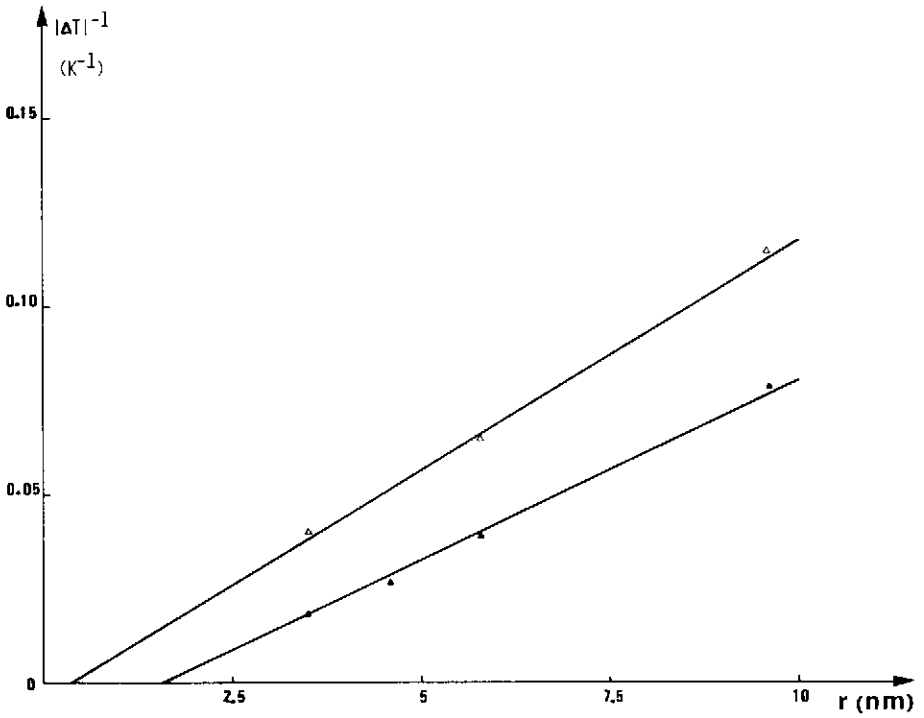

Fig. 9. Depression of the freezing point of hexane (△) and carbon tetrachloride (▲) as a function of the pore radius.

reactivated when the temperature is increased, their disappearance remains controlled by the surface tension γ_{ls} and by the average curvature of the solid matrix condensate interface.

III.4. Determination of pore radii distribution by calorimetry

III.4.1. Theoretical aspects of thermoporometry

When the thermograms extend over a broad temperature interval, it is not possible to consider ΔS_S and γ_{sl} as constant with respect to the temperature and to the capillary pressure of the liquid condensate. Calorimetric determination of the heat evolved during solidification makes it possible to calculate the volume V_n of the condensate which undergoes the change of state inside the porous material. V_n is given by the following equation:

$$[\Delta V_n]_r^{r+\Delta r} = \frac{[\Delta Q]_T^{T+\Delta T}}{W_S} v_l \tag{10}$$

The molar heat of solidification W_S is the sum of the heat of solidification of the bulk phase W_S' and of the heat W_S'' corresponding to the change of the liquid–solid matrix interface into a solid–solid matrix interface

$$W_S = W_S' + W_S'' \tag{11}$$

It is also necessary to take into account the volume of the layer of thickness t of the capillary condensate which does not undergo a change of state. The apparent energy of change of state inside a cylindrical pore of radius r is then:

$$W_A = W_S\left(\frac{r-t}{r}\right)^2 = (W'_S + W''_S)\left(\frac{r-t}{r}\right)^2 \tag{12}$$

The first contribution is given by:

$$W'_S = T\Delta S_{S_0} - \int_{T_0}^{T} \frac{C_l - C_s}{T}\,dT$$

$$-2\int_0^{(\gamma_{ls}/r-t)} \left[\frac{v_s}{v_s - v_l}\left(\frac{\partial v_l}{\partial T}\right)_p - \frac{v_l}{v_s - v_l}\left(\frac{\partial v_s}{\partial T}\right)_p\right] d\frac{\gamma_{ls}}{r-t} \tag{13}$$

This is the heat of solidification of the fraction of condensate which is inside a cylinder (or a sphere) of radius $r_n = r - t$.

The second contribution W''_S can be deduced from the Gibbs–Duhem equation and Young formula for each interface

$$(\Delta S_S)_{sup.} \simeq -\frac{2v_l}{r_n}\frac{d\gamma_{sl}}{dT}$$

III.4.2. Experimental procedure

The numerical relationships between the pore radius and the diminution of the solidification temperature, for a given condensate, can be deduced theoretically from eqn. (7) or from measurements of ΔT for samples of known radii.

For water: $r = -\dfrac{64.7}{\Delta T} + 0.57$ nm

For benzene: $r = -\dfrac{132}{\Delta T} + 0.54$ nm

These relations are valid for both cylindrical pores or spherical cavities.

The apparent solidification energy W_A, which is determined by calorimetry, is smaller than the solidification enthalpy at the normal triple point temperature as shown in Fig. 10. The numerical relations are deduced theoretically from eqn. (12).

For water: $W_A = -5.56 \times 10^{-2}\Delta T^2 - 7.43\Delta T - 332$ kJ g^{-1}

For benzene: $W_A = -8.87 \times 10^{-3}\Delta T^2 - 1.76\Delta T - 127$ kJ g^{-1}

In order to perform thermoporometry a certain amount of material, the weight of which (0.02–2 g) depending on its nature and on the sensitivity of the calorimeter, is placed inside the sample holder.

The sample can be saturated by condensation after outgassing in vacuum

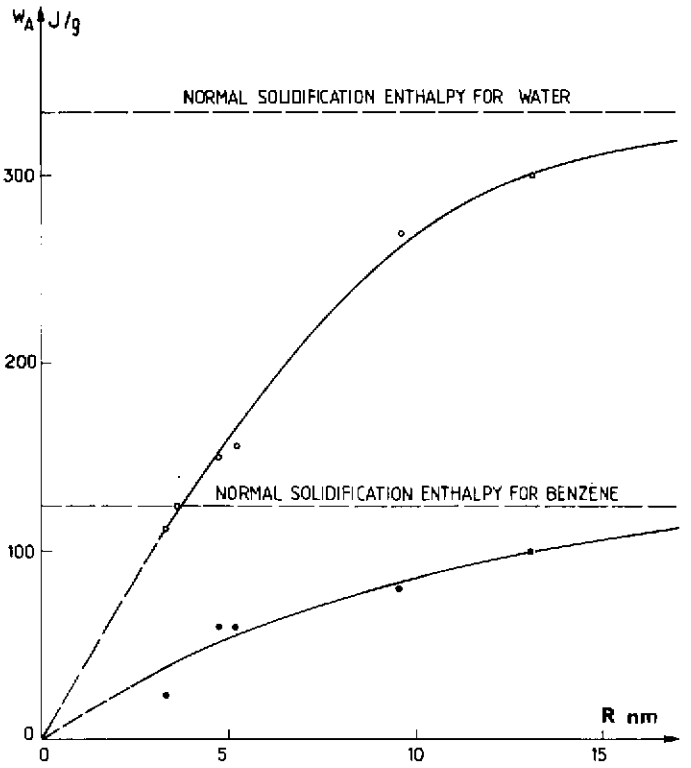

Fig. 10. Specific enthalpy of solidification of water and of benzene as a function of the pore radius.

but as it takes a long time, a simple method which gives the same result is used. It consists in dipping the oven-dried hot sample into the liquid.

The weight of condensate is determined precisely, the sample holder is sealed and placed inside a differential calorimeter. A linear decrease of temperature is programmed at a slow rate so that the three phases can be considered to be permanently in "equilibrium" (this equilibrium cannot be called thermodynamic as the state of the system is not the same during heating and cooling; the mechanical equilibrium of the surfaces is not reversible). The cooling rate is between 30 and 0.1 K h^{-1} depending on the thermal inertia of the calorimeter and on the size of the pores. The pore size distribution ($\Delta V/\Delta r = f(r)$) is deduced from the thermogram.

In the case of pore radii over 15.5 nm or of small amounts of sample or of some condensates supercooling, the measurement is difficult or even impossible.

In order to avoid this parasitic phenomenon, Brun and Quinson devised a method which consists of performing a first solidification followed by a slow increase of temperature up to the normal triple point temperature and in reprogramming the decrease in temperature before total melting of the

excess of condensate. The thermogram is recorded during the second cooling.

Some authors who have not realized this possibility use the melting thermogram but as mentioned before it is then necessary to make a hypothesis on the shape of the pores as in the case of the BJH method or mercury porometry [64].

III.5. Analysis of the thermogram

The method of analysis of the thermogram is illustrated by the curves in Fig. 11.

Curve (1) is the thermogram. Between t_1 and t_2, a fraction of the condensate is solidified, giving up an energy ΔW.

Curve (2) is the calibration curve giving the diminution $\Delta T = T - T_0$ of the freezing point of the liquids as a function of pore radius.

Curve (3) is the calibration curve giving the apparent energy of transformation per unit volume of liquid as a function of solidification temperature.

The thermogram is divided into intervals of 1 or 2°C, for each interval the following variables are tabulated.

T_i average freezing temperature corresponding to the interval pore radius
r_i average radius of the pore
Δr_i width of interval
ΔS_i area of the portion of thermogram in the interval
Wr_i volumic energy of solidification at temperature T_i
Δv_i pore volume within the interval
ΔV_i pore volume per unit mass of sample
$\Sigma \Delta V_i$ cumulative pore volume
$\Delta V_i / \Delta r_i$ volume frequency of pores of average radius r_i.

As this determination makes use of the calibration curves $\Delta T = f(r)$ and

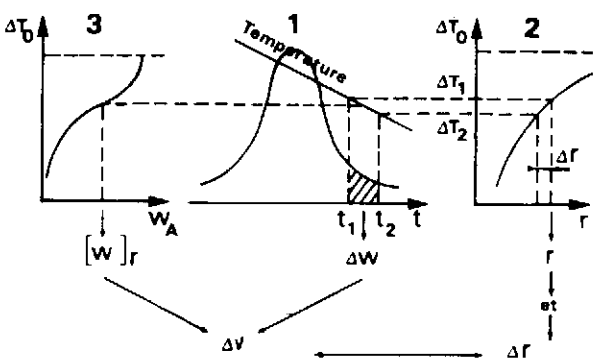

Fig. 11. Exploitation of a thermal analysis curve.

$W_S = f(\Delta T)$, this is only a relative method. It is possible to obtain an absolute value for the radius by using the equations of Laplace and Gibbs–Duhem for calculation of the solidification temperature (eqn. 6) and of the solidification enthalpy (eqn. 7). The parameters of these equations are now well known for water and benzene and it is no longer necessary to refer to calibration curves.

An automatic apparatus which can perform the analysis and the evaluation of the results has been built as a result of collaboration between CEA, CNRS and the University of Lyon I [65].

III.6. Examples of application

III.6.1. Divided and porous solids

Thermoporometry is a method which can be applied to a wide range of materials.

In the case of inorganic porous solids such as γ-alumina, the results are in good agreement with those obtained by mercury porometry or BJH porometry. When the pores cannot be considered as cylindrical, thermoporometry, which allows analysis of the pore section after section, gives higher values for the radius than the other methods.

Many of the physical properties of gels, and especially mechanical properties, are strongly dependent on the pore size and porosity. The porous distribution of silica gels prepared, for example, by hydrolysis of a solution of an organic silicon compound is usually destroyed when the gel is dried. Thermoporometry is the only method which can be used for analysing the texture of this material in the presence of the liquid phase [66,67].

Another example is the study of a porous organic resin (a copolymer of styrene and divinylbenzene). This resin can be used as a support catalyst in the liquid phase. Since it swells when put into the medium used, thermoporometry is the only method possible. BJH porometry performed on a resin reticulated enough to be lyophylized without much deformation compares favourably with the results of thermoporometry [68].

III.6.2. Membranes

Organic membranes for ultrafiltration, haemodialysis or dialysis prepared by a gelification process followed by coagulation are difficult to study. They are very often asymmetrical and the porous volume of the separative layer is very small.

In the case of the Rhône–Poulenc IRIS 3038 membrane thermoporometry shows pores of sizes within the range 5.4–110 nm. This very large pore size distribution is due to the method of preparation which must give a high permeability [69]. The smaller pores are formed inside the separation layer.

For the IRIS 3069 membrane, which mainly contains mesopores [69], the

results of thermoporometry have been compared with the retention curve determined by the calibrated particles method.

IV. MOBILITY OF GAS PHASES, ADSORBATES AND CONDENSATES ACROSS INORGANIC MESOPOROUS MEMBRANES

The percolation of a gas or of a mixture of gases through a mesoporous filter, when the pressure and temperature conditions allow adsorption or capillary condensation, gives rise to many theoretical problems. We mainly worked on three of them:

(1) The occurrence of a molecular flow in adsorbed phase, in the case of a single component.

(2) The effect of adsorption on separation in the case of a mixture of two isotopes.

(3) The calculation of the various resistances to the flow of the capillary condensate.

IV.1. Mobility of the adsorbed phase

The permeability to an adsorbable gas 1 of molar mass m_1 may be expressed by the sum of two terms. One comes from the flow in adsorbed phase, the other one from the flow in gas phase:

$$K_1 = K_{1\,\text{ads}} + K_{1\,\text{gas}}$$

The presence of the adsorbed phase plays a part on the gas phase flow by reducing the pore radius. In order to determine $K_{1\,\text{gas}}$ the adsorbable gas 1 is mixed with a non-adsorbable gas 2 of molar mass m_2 in such conditions that the partial pressure of gas 1 is very low and that the pressure difference between the two sides of the membrane also remains low. The second gas is helium. $K_{1\,\text{gas}}$ is deduced from the equation:

$$\frac{K_{1\,\text{gas}}}{K_2} = \sqrt{\frac{m_2}{m_1}}$$

Experimental measurements show that when the surface coverage is less than a monolayer $K_{1\,\text{ads}}$ can be expressed with a surface diffusion coefficient which is a function of the surface coverage [70].

IV.2. Isotopic separation by combined vapour adsorbate and condensate flow

The efficiency of the separation of argon isotopes by diffusion through a membrane of pore radius 4.2 nm has been studied as a function of the relative pressure of the gas. The main results are the following [71]:

(1) For a coverage less than a monolayer the adsorbate flow gives a

separation efficiency similar to a molecular rate of flow.

(2) Multilayer adsorption is unfavourable for separation by gaseous diffusion.

(3) When capillary condensation takes place the conditions of separation are the conditions of liquid–vapour equilibrium at the opening of the pores. Transfer through the membrane in this case leads to an enrichment in heavy elements instead of light elements.

IV.3. Resistance to the transfer of capillary condensates through a membrane

Transfer through a membrane of a gas in the form of a capillary condensate is controlled by four resistances:

(1) the resistances due to condensation at the gas–liquid meniscus upstream.

(2) the resistance to the flow of liquid condensate.

(3) the resistance due to evaporation of the liquid–gas meniscus downstream.

(4) the resistance to the gas flow downstream.

The mass flow is associated with a heat flow due to the capillary condensation and evaporation. The temperature gradient accounts for the difference in curvature of the meniscus upstream and downstream (Fig. 12).

The purpose of this study [72,73] was on the one hand the modellization of the transfer phenomenon in order to calculate the various resistances and on the other hand the measurement of the temperature difference between the upstream and downstream meniscus.

The transfer of Freon 11 through an alumina composite filter in which the mesoporous layer presents a pore radius of 9.3 nm makes it possible to work out the adjustable parameters of the model. In the specific case where the

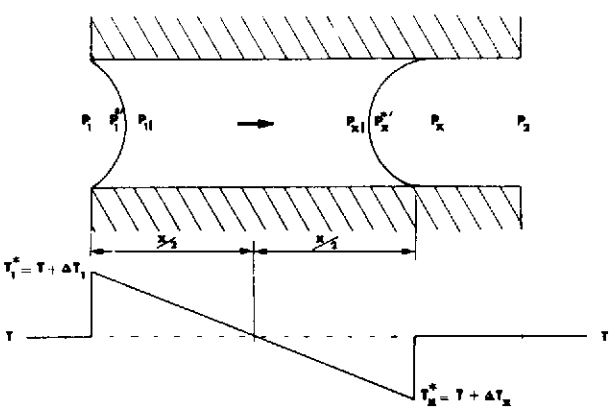

Fig. 12. Temperature profile between the entrance (condensation) and the exit (evaporation) of a pore.

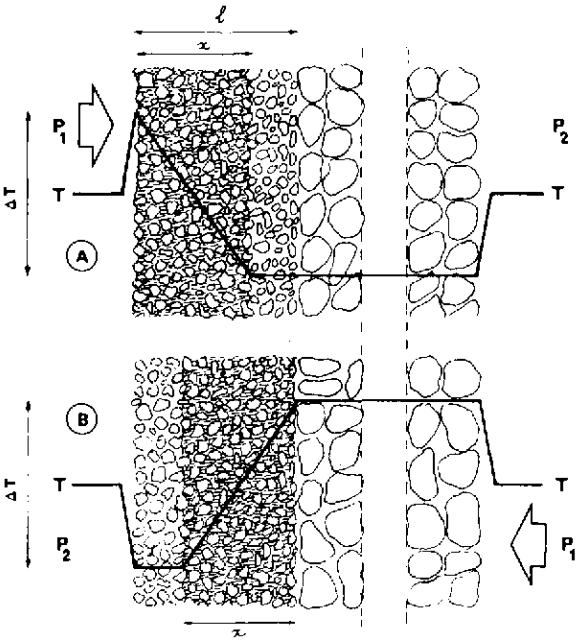

Fig. 13. Temperature profile between the condensation side and the evaporation side of an asymmetrical membrane. (A) Flow from the mesoporous layer towards the macroporous layer, (B) flow from the macroporous layer towards the mesoporous layer.

condensate fills up the mesoporous volume, it is shown that the transfer is controlled by the condensation and evaporation rates. The resistance due to a change of state is 50 times higher than the resistance due to the viscosity of the liquid condensate, it is 8 times higher than that due to the temperature difference upstream and downstream.

The temperature profile between the gaseous phases upstream and downstream is given in Fig. 13 in the case in which the vapour flows from the mesoporous side towards the support and in the case in which the vapour flows in the opposite direction. It is possible to measure the temperature gradient in the layer of liquid condensate by using two identical cylindrical

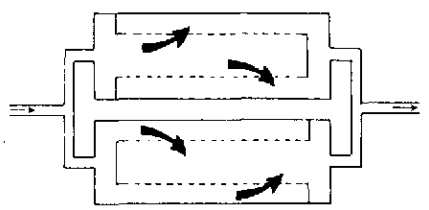

Fig. 14. Circulation of the vapour through two porous elements assembled as a differential flux meter.

elements with external mesoporous layer, assembled in parallel as in Fig. 14. The temperature difference between the external sides of the elements is measured by two coils of platinum wire in a Wheatstone bridge. It is between 0.5 and 2×10^{-2} K for a flow rate between 0.57×10^{-2} and 2.3×10^{-2} mol m^{-2} s^{-1}.

V. PERMPOROMETRY

V.1. Theoretical background

High permeability inorganic membranes for ultrafiltration are made of two or many porous layers, either superposed (Fig. 15a) or overlapping (Fig. 15b). In order to characterize the texture of the separative layer, supposed to be uniform, of a ceramic membrane of type (a), it is possible to sample scraps from the layer, and to submit them to one of the following methods: mercury porometry, BJH porometry, thermoporometry. In the case of structure (b), these three methods are unworkable, for the following three reasons:

(1) the mesoporous stuffings are not of uniform texture;
(2) they are difficult to sample;
(3) their relative volume is too small.

One is then led to resort to non-destructive dynamic techniques allowing characterization of a membrane as such. These techniques are bi-liquid permporometry and gas–liquid permporometry [74].

The former is based upon the Laplace relation ruling the mechanical equilibrium at the interface:

$$\Delta p = \frac{2\sigma}{r} \tag{14}$$

The experiment consists, for instance, in measuring the water flow rate through a membrane impregnated with isobutanol as a function of the pressure difference Δp.

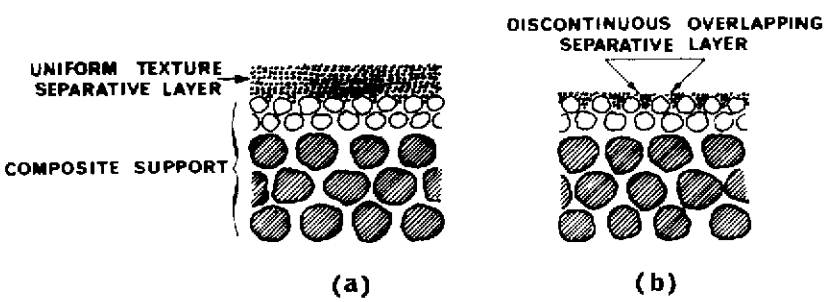

Fig. 15. Asymmetric membranes.

The latter is based upon the Kelvin relation ruling the liquid–vapour thermodynamic equilibrium of a capillary condensate:

$$\ln = \frac{p}{p_0} = -\frac{2\sigma}{r}\frac{v}{RT} \tag{15}$$

The experiment consists, for instance, in measuring the flow rate of helium containing a minute amount of a condensable vapour like ethanol, as a function of the relative pressure of this vapour. The gas flow regime is of Knudsen type in all open pores. Both methods allow the membrane permeability K to be expressed as a function of the pore radius, either as a cumulative value $K = \mathrm{f}(r)$ or as a differential one $\Delta K/\Delta r = \mathrm{g}(r)$.

We have been more especially interested in the latter method. It has the advantage of not accumulating any pollutants at the level of the separative layer which would induce changes in the liquid–liquid interfacial energy and in the three phase contact angle. The ideas were those of Eyraud [74] and of Katz [75]. They corresponded to a stationary flow regime. However, they suffered from many drawbacks:

(1) measurement of small gas flows is difficult, especially over a wide variation interval;

(2) it is not easy to realize a feed at variable flow of a gaseous mixture containing a vapour at a relative pressure very precisely known at the vicinity of $p/p_0 = 1$;

(3) at high relative pressures, the intervention of a capillary flow of condensate induces a relatively important decrease of condensable gas on the inlet side.

This is why we chose a pseudo-stationary technique [76–78], depicted by Fig. 16, that we named "gas–liquid permporometry".

V.2. Gas–liquid permporometry

A membrane of area A has two closed compartments, of respective volumes V_1 and V_2, about 1 l each. Volume V_1 is connected to bellows made of corrugated metal, with a reciprocating motion of volumetric amplitude of about 1 cm^3, and of pulsation ω. The membrane is previously brought to equilibrium with vapour by helium circulation between an ethanol evaporator at temperature T and the membrane holder at temperature T_0. If T_A is the ambient temperature, condensation in the tubings is avoided by complying with the condition $T < T_A$. When the four valves are closed, the phase differense ϕ between the variation of volume V_1 and the pressure difference between the two compartments is expressed by the relation:

$$\omega \tan \phi = AKRT_0\left(\frac{1}{V_1} + \frac{1}{V_2}\right) \tag{16}$$

A, ω, V_1 and V_2 are known. The permeability K is deduced from the

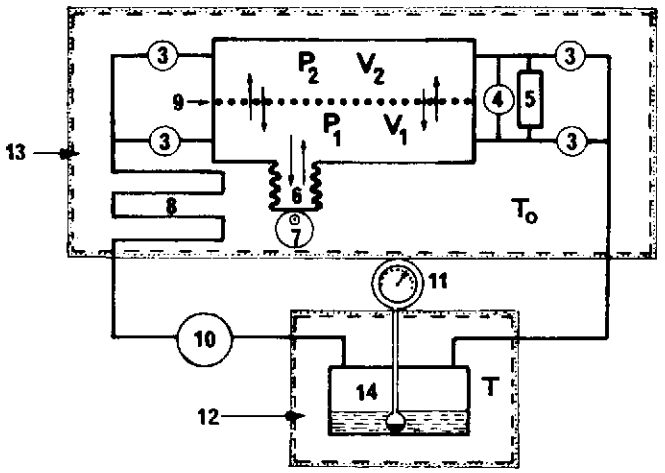

Fig. 16. Gas–liquid permporometer. (V_1), (V_2) gas compartments, (3) electrovalves, (4) by-pass, (5) differential pressure detector, (6) bellow metal, (7) cam, (8) heat exchange, (9) ultrafilter, (10) metallic membrane pump, (11) absolute pressure manometer, (12) enclosure thermoregulated at temperature T, (13) enclosure thermoregulated at temperature T_0, (14) ethanol evaporator.

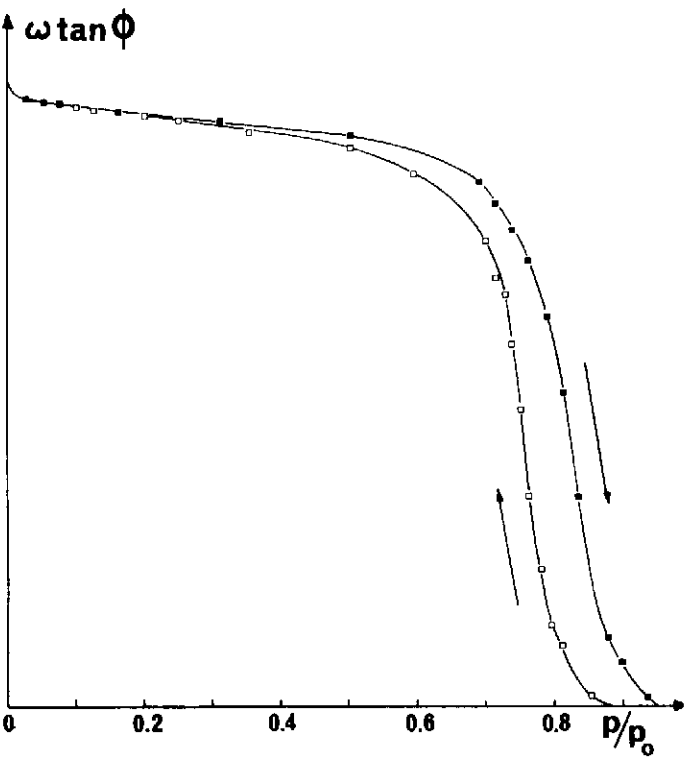

Fig. 17. Phase difference between the variation of volume V_1 and the variation of pressure P_2 as a function of the relative vapour pressure.

measurement of ϕ. Thus, the variation of $\omega \tan \phi$ versus p/p_0 can be represented by the curve in Fig. 17. The distribution $K_k = f(r_k)$ can be deduced by taking into account the relations (15) and (16). To improve the method, it is necessary to take into account the thickness of the layer of molecules adsorbed at the surface of open pores. The actual pore radius r_p is related to the Kelvin radius r_k by:

$$r_p = r_k + en \tag{17}$$

where e is the unimolecular layer thickness ($e = 0.44$ nm for ethanol) and n is the number of layers given by the Halsey relation:

$$n = \left(\frac{B}{\ln p/p_0} \right)^{1/x} \tag{18}$$

B and x result from experimental determinations carried out for the adsorbate–adsorbent couple, outside the domain of capillary condensation. This is the way in which the distribution curve of Fig. 18 is obtained. The permporometry radius at 50% of membrane permeability is $r_{pp50} = 5.5$ nm; the permporometry radius at maximum of distribution curve, $\Delta K_p/\Delta r_p = g(r_p)$, is $r_{ppmax} = 5.2$ nm.

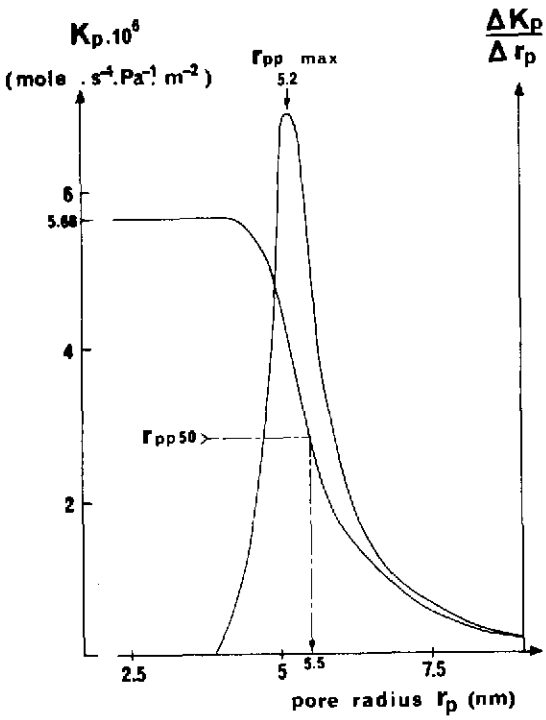

Fig. 18. Permeability distribution as a function of the pore radius (cumulative and differential curves).

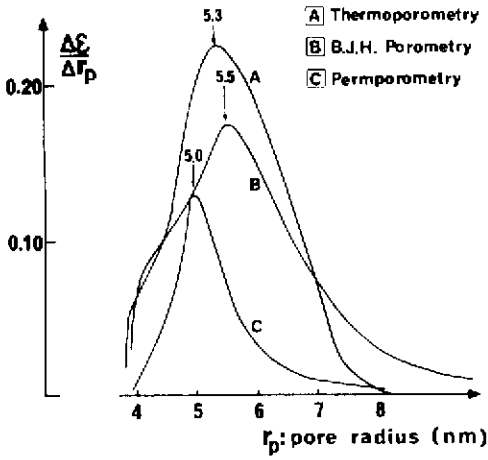

Fig. 19. Porosity distribution as a function of the pore radius.

In order to check this method, we resorted to a cylindrical composite alumina ultrafilter, of the type depicted in Fig. 15a. The separative layer is considered to be of uniform texture, and of exactly known thickness. The support permeability is at least one hundred times larger than that of the fine layer. By assuming for the latter a model of cylindrical pores perpendicular to the membrane sides, it is possible to pass from the permeability distribution $\Delta K_p/\Delta r_p = g(r_p)$ to the porosity distribution $\Delta\epsilon/\Delta r_p = h(r_p)$. We write that the class of pores of Kelvin radius r_k takes part in permeability with the value:

$$dK_k = s\frac{dN}{l}\frac{2\Pi}{MRT_0}r_k^3 \tag{19}$$

where l is the thickness of the separative layer, N the number of pores per surface unit. It is assumed that the gliding coefficient at the wall s is equal to 1.

Figure 19 represents the pore size distribution obtained by the three following methods:

(1) thermoporometry, effected on scraps of the separative layer;

(2) BJH porometry. In this case, the isotherm of nitrogen desorption at liquid nitrogen temperature is obtained by thermogravimetry;

(3) helium–ethanol permporometry, effected on a complete membrane.

CONCLUSIONS

This article summarizes the scientific results obtained by the research workers with whom I had the pleasure and the privilege to collaborate. Most of the references are related to research programmes to which I have been

associated or to techniques I contributed to developing or improving. A more comprehensive bibliographic analysis can be found in the articles cited and in the general articles written by the researchers in my laboratory which were published in "Techniques de l'Ingénieur" under the thermal methods rubric: thermogravimetry [14], microcalorimetry (M. Brun and P. Claudy), dilatometry (M. Murat) solid thermoconductimetry (E. Karmazsin).

Lyon's industry has been contributing to the development of thermal methods for a long time. The first thermobalance which was marketed was devised by Talabot in 1833. From 1853 to 1854, 42 specimens were manufactured, they were used by one of Lyon's companies "La Condition des Soies" to measure the moisture content of silk bales from China [79] in order to set the price (Fig. 20).

The first microcalorimeter marketed was built by Setaram Company in 1961 according to the principle of Tian and Calvet. Since then, this company has been using the results of the scientists of the "Institut de Recherches sur la Catalyse", "Institut National des Sciences Appliquées" and "Université

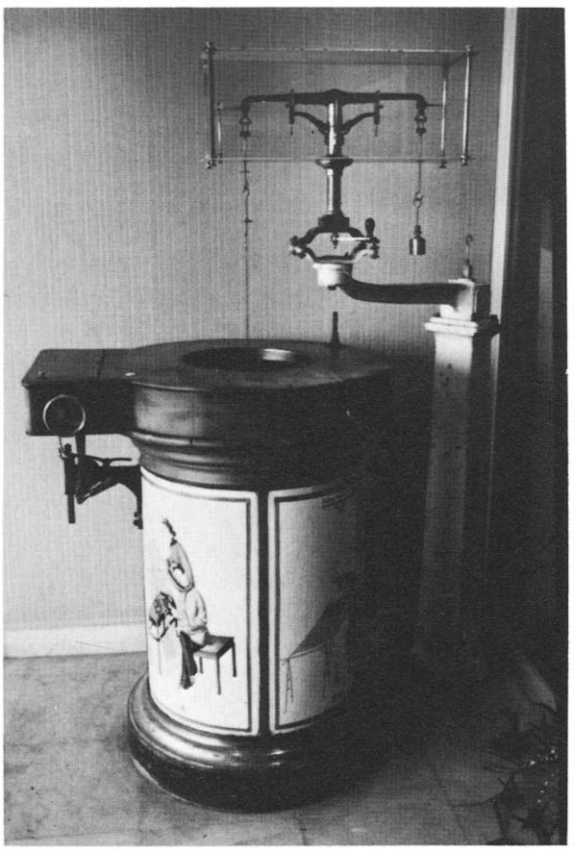

Fig. 20. Talabot's thermobalance.

Claude Bernard" in Lyon, to devise and market new apparatuses in thermogravimetric and quantitative differential thermal analysis.

The work presented here was carried out with a constant concern for the needs of industry without neglecting fundamental research.

The "Commissariat à l'Energie Atomique" have helped us in our efforts to reach this double aim for several years. Among those who constantly gave us their financial and intellectual support we particularly wish to thank C. Frejacques (Membre de l'Institut, Président du Centre National de la Recherche Scientifique) and P. Plurien (Chief of Isotopic Engineering Department of C.E.A.).

REFERENCES

1 C. Eyraud and L. Eyraud, Cataloque Exposition Soc. Fr. Phys. Paris, (1953) 163.
2 C. Eyraud and I. Eyraud, Laboratoire, 12 (1955) 13.
3 E. Robens, M. Escoubes and C. Eyraud, Thermochim. Acta, 82 (1984) 15.
4 C. Eyraud and R. Goton, J. Chim. Phys., 51 (1954) 430.
5 F. Corbet and C. Eyraud, Bull. Soc. Chim. Fr., (1961) 571.
6 P. Turlier, L. Eyraud, C. Eyraud and M. Prettre, C.R. Acad. Sci., 246 (1958) 422.
7 M. Escoubes and C. Eyraud, Bull. Soc. Chim. Fr., 4 (1969) 1369.
8 M. Escoubes, J.F. Quinson and C. Eyraud, Bull. Soc. Chim. Fr., 7 (1967) 2435.
9 J.C. Volta, P. Turlier and Y. Trambouze, J. Catal., 34 (1974) 329.
10 M. Gery, M.A. Michou-Saucet, J. Lenoir, P. Pierron and C. Eyraud, C.R. Acad. Sci., 254 (1962) 688.
11 M. Mange, J.L. Thomas and C. Eyraud, Bull. Soc. Chim. Fr., 10 (1969) 3375.
12 L. Tournayan, H. Charcosset, R. Frety, C. Leclercq, P. Turnier, J. Barbier and G. Leclercq, Thermochim. Acta, 27 (1978) 95.
13 M. Baggioni, P. Eyraud and C. Eyraud, Le Vide, 102 (1962) 565.
14 C. Eyraud, M. Cronenberger and M. Cognat, Collections Techniques de l'Ingénieur, printed by Imprimerie Strasbourgeolse (Strasbourg). Mesures et Analyse: Thermogravimétrie, Vol. P 880 (1962) pp. 1–13.
15 P. Gonnard, C. Bardot et C. Eyraud, Chim. Ind. Génie Chim., 102 (1969) 645.
16 M. Mange, F. Chatelut et C. Eyraud, J. Appl. Chem. Biotechnol., 27 (1977) Pap. 234.
17 P. May, Thesis, Lyon, 1967.
18 R. Spitz and P. Turlier, J. Chim. Phys., 66 (1969) 1256.
19 J.C. Volta and P. Turlier, J. Chim. Phys., 71 (1974) 1263.
20 V. Perrichon, J. Vialle, P. Turlier, G. Delvaux, P. Grange and B. Delmont, C.R. Acad. Sci., Ser. C, 282 (1976) 85.
21 M. Escoubes and M. Karchoud, Bull. Soc. Fr. Ceram., (1977) 43.
22 M. Escoubes, J.F. Quinson, J. Gielly, and M. Murat, Bull. Soc. Chim. Fr., 5 (1972) 1689.
23 R. Blanc and M. Escoubes, Thermochim. Acta, 11 (1975) 115.
24 J.F. Quinson, M. Escoubes and R. Blanc, Bull. Groupe Fr. Argiles, 24 (1972) 49.
25 Briner et al., Helv. Chim. Acta, 19 (1936) 308, 320, 1074; 21 (1938) 134; 22 (1939) 1096; 25 (1942) 530, 889; 28 (1945) 714.
26 C. Eyraud, C.R. Acad. Sci., 225 (1947) 679.
27 C. Eyraud, Thesis, Lyon, 1950.
28 J. Janin and C. Eyraud, Rev. Otique, 28 (1949) 612.
29 P. Bussiere, B. Domenski, C. Eyraud and M. Prettre, C.R. Acad. Sci., 243 (1956) 1870.
30 P. Devore, C. Eyraud and M. Prettre, C.R. Acad. Sci., 246 (1958) 1200.

31 C. Eyraud et al., C.R. Acad. Sci., 242 (1956) 905.
32 C. Eyraud et al., C.R. Acad. Sci., 258 (1964) 5860; 261 (1965) 1291.
33 C. Lormand, J.C. Rouais, M. Lallemand and C. Eyraud, Mém. Sci. Rev. Métall., 64 (1967) 59.
34 G. Lormand, J.C. Rouais and C. Eyraud, Acta Metall., 22 (1974) 793.
35 G. Lormand et al., C.R. Acad. Sci., Ser. B, 274 (1972) 827; Ser. C, 274 (1972) 940; Ser. B, 276 (1973) 385.
36 C. Eyraud, R. Goton, Y. Trambouze, T.H. The and M. Prettre, C.R. Acad. Sci., 240 (1955) 862.
37 P. Lokodey, C. Eyraud and M. Prettre, C.R. Acad. Sci., 242 (1956) 3071.
38 G. Boutillon, C. Eyraud and M. Prettre, C.R. Acad. Sci., 240 (1955) 756.
39 C. Eyraud, Technica, 177 (1954) 2.
40 J.L. Petit, L. Sicard and L. Eyraud, C.R. Acad. Sci., 252 (1961) 1740.
41 C. Berger, M. Richard and L. Eyraud, Bull. Soc. Chim. Fr., (1965) 1491.
42 L. Eyraud, Diélectriques Solides Anisotropes et Ferroélectricité, Gauthier Villars, Paris, 1967.
43 R. Reynaud, M. Bernard, M. Richard, L. Eyraud and J. Elston, Mach. Outil Fr., 206 (1965) 57.
44 A. Roux, M. Richard, L. Eyraud and J. Elston, J. Phys. Appl., 25 (1964) 51A.
45 A. Roux, Thesis, Lyon, 1969.
46 L. Sicard, L. Eyraud, G. Malecot, J. Elston and C. Eyraud, C.R. Acad. Sci., 248 (1959) 2970.
47 H. Kleimann, Y. Fetiveau, M. Richard, L. Eyraud and C. Eyraud, Rapp. CEA-R-3644 (1969) 1.
48 L. Sicard, L. Eyraud and J. Elston, C.R. Acad. Sci., 249 (1959) 642.
49 L. Sicard, L. Eyraud, J. Elston and C. Eyraud, J. Phys Radium, 21 (1960) 696.
50 G. Berthier and L. Sicard, C.R. Acad. Sci., 258 (1964) 483.
51 G. Berthier, Thesis, Lyon, 1964.
52 B. Rasneur, G. Schnedecker and J. Charpin, Silic. Ind., (1972) 1301.
53 B. Rasneur, Bull. Soc. Fr. Ceram., 101 (1973) 21.
54 M. Büchwer, E. Robens and R.Sh. Mikhail, in C. Eyraud and M. Escoubes (Eds.), Progress in Vacuum Microbalance Techniques, Heyden, London, Vol. 3, 1975, pp. 324–329.
55 R. Defay and I. Prigogine, Tension Superficielle et Adsorption, Desoer, Liège, 1951.
56 M. Brun, Thesis, Lyon, 1973.
57 M. Brun, A. Lallemand, J.F. Quinson and C. Eyraud, Thermochim. Acta, 21 (1977) 59.
58 C. Eyraud, Summer School on Membrane Processes, Cadarache, France, 1984.
59 M. Brun, A. Lallemand, J.F. Quinson and C. Eyraud, J. Chim. Phys., 70 (1973) 973.
60 M. Brun, J.F. Quinson, B. Martini and C. Eyraud, J. Chim. Phys., 75 (1978) 469.
61 J.F. Quinson, M. Brun, A. Lallemand and C. Eyraud, C.R. Acad. Sci., Ser. B, (1967) 405.
62 A. Lallemand, J.F. Quinson, M. Brun and C. Eyraud, C.R. Acad. Sci., Ser. B, (1975) 329.
63 J.F. Quinson, M. Brun and M. Roubin, J. Therm. Anal., 20 (1981) 389.
64 L.G. Homshaw, J. Colloid Interface Sci., 84 (1981) 141.
65 P. Barberi, P. Bergez, M. Brun, M. Chevalier, C. Eyraud and J.F. Quinson, French patent 8 414 792 (1984).
66 S. Baza, Thesis, Lyon, 1984.
67 J.F. Quinson, J. Dumas and J. Serughetti, J. Non-Cryst. Solids, 79 (1986) 397.
68 M. Brun, J.F. Quinson, R. Spitz and M. Bartholin, Makromol. Chem., 183 (1982) 1523.
69 J. Desbrieres, M. Rinaudo, M. Brun and J.F. Quinson, J. Chim. Phys., 78 (1981) 187.
70 A. Lallemand and C. Eyraud, Bull. Soc. Fr. Ceram., 99 (1973) 25.
71 A. Lallemand and C. Eyraud, Bull. Soc. Fr. Ceram., 100 (1973) 31.
72 R. Frigiere, Thesis, Lyon, 1979.

73 R. Frigiere and C. Eyraud, Bull. Soc. Chim. Fr., 11-12 (1983) I.300.
74 C. Eyraud, J. Bricout and G. Grillet, C.R. Acad. Sci., 257 (1963) 2460.
75 M.G. Katz, World Filtration Congress III, Downingtown, PA, 1982, p. 508.
76 S. Bienfait, Thesis, Lyon, 1967.
77 C. Eyraud, M. Betemps, J.F. Quinson, F. Chatelut, M. Brun and B. Rasneur, Bull. Soc. Chim. Fr., 9–10 (1984) I.237.
78 C. Eyraud, Europe–Japan Congress on Membrane and Membrane Processes, Stresa, Italy, 1984.
79 A. Perret, Monographie de la Condition des Soies, Edited by Chambre de Commerce de Lyon, Imprimerie Pitrat Ainé, Lyon, 1878.